

Highly Undersampled MRI Reconstruction via a Single Posterior Sampling of Diffusion Models

Jin Liu, Qing Lin, Zhuang Xiong, Shanshan Shan, Chunyi Liu, Min Li, Feng Liu, G. Bruce Pike, *Senior Member, IEEE*, Hongfu Sun, Yang Gao

Abstract—Incoherent k-space under-sampling and deep learning-based reconstruction methods have shown great success in accelerating MRI. However, the performance of most previous methods will degrade dramatically under high acceleration factors, e.g., $8\times$ or higher. Recently, denoising diffusion models (DM) have demonstrated promising results in solving this issue; however, one major drawback of the DM methods is the long inference time due to a dramatic number of iterative reverse posterior sampling steps. In this work, a Single Step Diffusion Model-based reconstruction framework, namely SSDM-MRI, is proposed for restoring MRI images from highly undersampled k-space. The proposed method achieves one-step reconstruction by first training a conditional DM and then iteratively distilling this model. Comprehensive experiments were conducted on both publicly available fastMRI images and an in-house multi-echo GRE (QSM) subject. Overall, the results showed that SSDM-MRI outperformed other methods in terms of numerical metrics (PSNR and SSIM), qualitative error maps, image fine details, and latent susceptibility information hidden in MRI phase images. In addition, the reconstruction time for a 320×320 brain slice of SSDM-MRI is only 0.45 second, which is only comparable to that of a simple U-net, making it a highly effective solution for MRI reconstruction tasks.

Index Terms—MRI Acceleration, Single-Step Diffusion Model (SSDM), QSM Acceleration, Image Reconstruction

I. INTRODUCTION

MAGNETIC Resonance Imaging (MRI) is a non-invasive and radiation-free imaging modality that has been widely used in clinical diagnosis and research [1], [2] thanks to its excellent tissue contrasts and high image resolutions. However, MRI acquisitions are relatively slow since large areas of k-space need to be traversed, which not only leads to patient discomfort, but also increases the risk of motion artifacts.

Incoherent undersampling combined with compressed sensing (CS) reconstruction algorithms has been substantially studied to accelerate MRI scans, by solving an ill-posed inverse problem. Many traditional iterative reconstruction algorithms

YG acknowledges the supported from the National Natural Science Foundation of China under Grant No. 62301616, 62301352, and the Natural Science Foundation of Hunan (Grant No. 2024JJ6530). GBP acknowledges support from the Canadian Institutes for Health Research (CIHR-FDN 143290). HS thanks the support from the Australia Research Council (DE20101297 and DP230101628), and National Health and Medical Research Council of Australia (Grant No. 2030157).

J. Liu, Qi. Lin, M. Li, and Y. Gao are with school of computer science and engineering, Central South University, China. Z. Xiong is with School of Health Sciences, Faculty of Medicine and Health, University of Sydney, Australia. S. Shan is with State Key Laboratory of Radiation, Medicine and Protection, Soochow University, Suzhou, China. C. Liu is with Medical School, Nanjing University, China. F. Liu is with School of Electrical Engineering and Computer Science, University of Queensland, Brisbane, Australia. G.B. Pike is with Departments of Radiology and Clinical Neurosciences, Hotchkiss Brain Institute, University of Calgary, Calgary, Canada. H. Sun is with School of Engineering, University of Newcastle, Newcastle, Australia. Corresponding Author: Yang Gao (yang.gao@csu.edu.cn).

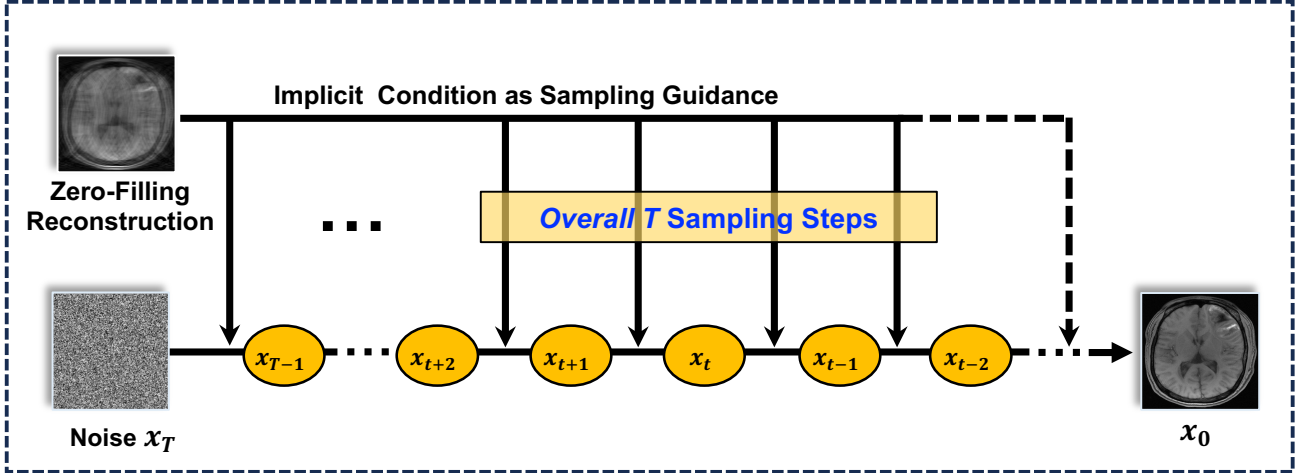
have been developed since the pioneering work of Lustig [3], [4], such as image sparsity-based CS methods [3]–[7] or low-rankness models [8]–[10]. However, the performance of these algorithms will substantially decrease at high acceleration factors, leading to image blurring or residual artifacts. In addition, they are usually computationally expensive and require manual hyperparameter tuning [11].

Deep learning (DL) algorithms have been increasingly popular as an alternative to conventional iterative methods for MRI acceleration. Many end-to-end supervised deep neural networks [12]–[15], such as U-net [16] based methods, have been proposed for MRI reconstruction recently, demonstrating better artifact removal and improved fine details, compared with traditional iterative methods. However, the generalization capability of these methods is limited, and their performance will degrade when applied to data out of the training distribution. Whereas, unrolling-based or model-based deep neural network [17], [18] is another framework incorporating physical models in deep neural network designs, demonstrating better results as well as generalization capability. However, these two frameworks will both decrease their performance when applied to highly undersampled k-space data (e.g., $8\times$ or higher).

Recently, diffusion models (DM) [19]–[23] or noise-conditioned score networks are increasingly popular for MRI reconstruction at high acceleration factors [24]–[33]. This new framework holds great potential for achieving ultra-high k-space acceleration factors, as long as a desirable generative model is successfully trained, which allows high-quality MRI synthesis from only random noise. However, a dramatic number of iterative reverse posterior sampling steps are usually necessary for DM to generate reliable results, which will accumulate reconstruction times, making DM-based MRI reconstruction framework much slower than previous DL methods, e.g., end-to-end network-based methods [12]–[14].

In this work, a Single Step Diffusion Model-based method, namely SSDM-MRI, is designed to reconstruct MRI images from highly subsampled k-space in just one posterior sampling step, thus enabling much faster computation than conventional DM-based methods. The proposed method was developed by progressively distilling a pre-trained conditional DM, which was obtained through a supervised learning scheme to enhance the stability and controllability. Comprehensive experiments were conducted on both the public fastMRI brain and knee datasets [34] and an in-house complex-valued brain dataset to compare the proposed SSDM-MRI with multiple established MRI reconstruction methods, including both iterative algorithms and deep learning frameworks. The performances of SSDM-MRI at different acceleration rates were also investigated. In addition, we also evaluated SSDM-MRI's performance on Quantitative Susceptibility Mapping (QSM) accel-

(a) Conventional Reverse Diffusion Sampling



(b) Single-Step Diffusion Model-based MRI Reconstruction

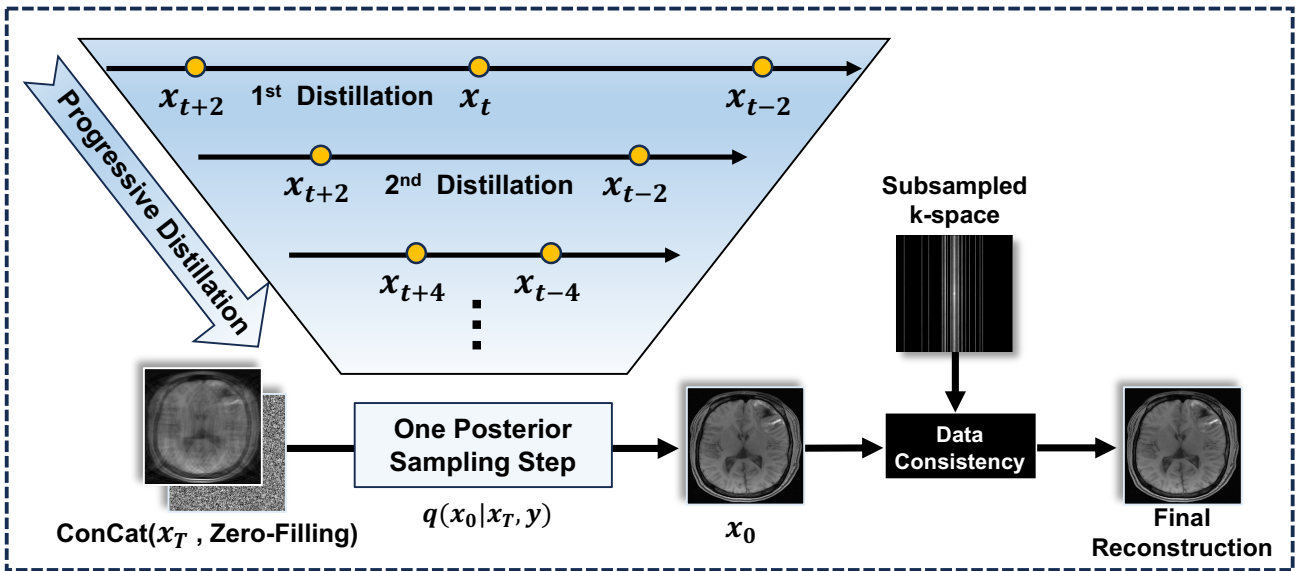


Fig. 1. Overall framework of the proposed Single-Step Diffusion Model-based MRI reconstruction (SSDM-MRI) method, which is developed by iteratively distilling a pre-trained conditional diffusion model to reduce necessary number of reverse sampling steps from original T times to just one step.

eration task using the in-house brain dataset.

II. THEORY AND RELATED WORKS

A. Problem Formulation

MRI reconstruction from subsampled k-space data can be formulated as:

$$\mathbf{y} = \mathbf{A}\mathbf{x} + \boldsymbol{\epsilon}, \quad (1)$$

where $\mathbf{y} \in \mathbb{C}^m$ represents the undersampled k-space measurements and $\mathbf{x} \in \mathbb{C}^n$ is the underlying image, and $m \ll n$; $\boldsymbol{\epsilon} \in \mathbb{C}^m$ is the measurement noise, and $\mathbf{A} \in \mathbb{C}^{m \times n} = \mathbf{M} \times \mathbf{F}$ represents the system forward model, with $\mathbf{M} \in \mathbb{C}^{m \times n}$ being the undersampling mask and \mathbf{F} as the Fourier transform. Equation (1) is also known as the general forward model of MRI reconstruction, serving as a training data generator in many supervised learning frameworks [14], [35], [36].

B. Conventional Iterative and Deep Learning Algorithms

Equation (1) could be solved using the following optimization framework, which can be calculated iteratively:

$$\mathbf{x}^* = \underset{\mathbf{x}}{\operatorname{argmin}} f(\mathbf{A}\mathbf{x} - \mathbf{y}) + \lambda \mathfrak{R}(\mathbf{x}), \quad (2)$$

where $\mathbf{x} = m e^{i\theta}$; m is the magnitude images, and θ is the phase signals; $f(\cdot)$ is a loss function enforcing data fidelity, e.g., the commonly used l_2 norm; $\mathfrak{R}(\cdot)$ is a manually-designed regularization term, which can be a sparsifying transformation (e.g., Total Variation and Wavelet Transform), and λ is a weighting hyperparameter. In most previous studies [3], [37]–[39], the phase signal is simply estimated from the low-frequency part of k-space to simplify this problem; however, a complex phase regularizer is also necessary for phase-based advanced applications [15], [40], [41], e.g., Quantitative Susceptibility Mapping (QSM).

Deep neural networks, due to their excellent performances in complex feature representation capability compared with manually-designed regularizers (i.e., $\mathfrak{R}(\cdot)$ in Eq. (2)), have demonstrated improved reconstruction performances. End-to-end neural networks [12]–[14] and deep unrolling networks [17], [18] are two very commonly used frameworks in CS-MRI. The former can be briefly described as follows:

$$\mathfrak{N}_{\theta^*} = \underset{\theta}{\operatorname{argmin}} \sum_{n=1}^N f(\mathbf{x}_n - \mathfrak{N}_{\theta}(\mathbf{A}^H \mathbf{y}_n)) + \mathfrak{S}(\theta), \quad (3)$$

where θ is the learnable parameters in the deep network \mathfrak{N} , and $f(\cdot)$ is the loss function adopted for network training; $\mathfrak{S}(\theta)$ represents the techniques used to address the potential overfitting problems in deep and large models. In this scheme, end-to-end networks tried to directly learn the non-linear mapping between training inputs, which is usually the zero-filling reconstructions (i.e., $\mathbf{A}^H \mathbf{y}_n$), and training labels (\mathbf{x}_n). Whereas deep unrolling networks, on the other hand, are usually constructed by iteratively stacking physical-model modules and neural networks. The network part usually tries to learn the mapping between latent variables in conventional iterative algorithms (i.e., learning the proximal gradient descent process in ISTA-Net [18]).

C. Diffusion Models for MRI Reconstruction

Diffusion models (DM) [19], [21], [22] or the noise-conditioned score networks (NCSN) [20], [23] are new types of generative models that are capable of synthesizing high-quality images via gradually denoising Gaussian noise. It involves a forward noise adding process to convert the original image into pure Gaussian noise, and an iterative backward sampling process to recover the original images in T consecutive steps. DM is naturally suitable for solving inverse problems and has shown great potential in MRI reconstructions [24]–[31].

Suppose that the desired MRI images follow a specific unknown distribution (i.e., $\mathbf{x} \sim p(\mathbf{x})$), then the reconstruction of MRI images (\mathbf{x}) from subsampled k-space (\mathbf{y}) can be formulated as a posterior sampling process $p(\mathbf{x}|\mathbf{y})$, and the key to obtain reliable samples from this conditional distribution in the DM backward process is to estimate the corresponding score function $\nabla_{\mathbf{x}_t} \log(p(\mathbf{x}_t|\mathbf{y}))$ [20], [42] (i.e., the noise estimation in DM). One can train a deep neural network to estimate this conditional score ($\mathfrak{N}_{\theta}(\mathbf{x}_t, \mathbf{y}) \approx \nabla_{\mathbf{x}_t} \log(p(\mathbf{x}_t|\mathbf{y}))$) in a supervised or unsupervised manner.

D. Progressive Diffusion Model Distillation

One major drawback of DM-based methods is the slow sampling (backward) process, which usually takes a large number of posterior sampling steps. Distillation strategies were commonly employed to accelerate the posterior sampling process in many previous works [23], [43], among which progressive distillation [44] has been one of the most effective techniques. It iteratively reduces the number of necessary sampling steps by distilling a teacher diffusion model into a faster student model, which then becomes a new teacher for the next iterative distillation. Every distillation reduces the number of necessary sampling steps from T steps to $T/2$ steps.

A. Overall Framework of SSDM-MRI

The proposed SSDM-MRI takes the zero-filling reconstructions as well as the Gaussian noise as inputs (concatenated along the channel dimension), and generates desired MRI images as outputs, as demonstrated in Fig. 1. To achieve robust image reconstruction with only one posterior sampling, a conditional denoising diffusion probability model (DDPM) [45] was first trained using supervised learning, and it was then progressively distilled to speed up the sampling process, decreasing T necessary reverse sampling steps to only one step. Data consistency [15], [46] was also performed to further refine the DM-synthesised images to impose the k-space data fidelity, as described in Eq. (4) below:

$$\mathbf{x}_{dc}(\mathbf{k}) = (1 - M) \cdot \mathbf{x}_0(\mathbf{k}) + \mathbf{y}(\mathbf{k}), \quad (4)$$

where $\mathbf{x}_0(\mathbf{k})$ is the original diffusion model reconstructions in k-space, M is the undersampling mask, and $\mathbf{y}(\mathbf{k})$ is the subsampled k-space data. The final reconstruction of SSDM-MRI is the inverse Fourier Transform of k-space signal $\mathbf{x}_{dc}(\mathbf{k})$.

B. Diffusion Model Pretraining and Distillation

Similar to most previous works [19], [20], the forward process is a stable Markov chain of diffusion steps, gradually adding Gaussian noise into the fully-sampled MRI images (\mathbf{x}_0), which is controlled by a parameter scheduler $\{\gamma_t \in (0, 1), t = 1, 2, 3, \dots, T\}$. In this work, T was set as 128 and a cosine noise scheduler ($\gamma_t = \cos^2(\pi/2 * t/T)$) was adopted during DM pretraining, and the forward process can be expressed as follows:

$$\mathbf{x}_t = \sqrt{\gamma_t} \mathbf{x}_0 + \sqrt{1 - \gamma_t} \boldsymbol{\epsilon}, \quad \boldsymbol{\epsilon} \sim \mathcal{N}(0, \mathbf{I}), \quad (5)$$

where \mathbf{x}_t is the noise contaminated image at time step t , \mathbf{x}_0 is the noise free images, \mathbf{x}_T is pure Gaussian noise, and $\bar{\gamma}_t = \prod_{i=1}^t \gamma_i$.

The pre-trained conditional DM was obtained by training a self-tailored residual U-net (\mathfrak{N}_{θ}) on a large number of paired datasets ($\{(\mathbf{A}^H \mathbf{y})^n, \mathbf{x}_0^n\}_{n=1,2,3,\dots,N}$) simulated based on Eq. (1), as detailed in **Algorithm 1**. Overall, the U-net takes both \mathbf{x}_t and zero-filling reconstructions ($\mathbf{A}^H \mathbf{y}$) as its major inputs (concatenated along the channel dimension). Similar to most previous U-net models, this adopted U-net consists of an encoding and a decoding path, each consisting of three modules, and each module contains three convolutional blocks with residual connections from the block input to the output. Three pooling layers and three corresponding unpooling layers were included for multiscale or multi-resolution learning. Self-attention operations were only carried out on the latent features of the lowest resolution due to memory constraints. Overall, the network consists of 52 convolutional layers (kernel size: 3×3), 3 max-pooling layers (kernel size: 2×2), 3 transposed convolutional layers (kernel size: 2×2), 51 batch-normalization layers, 77 rectified linear units (ReLU), 3 concatenations, 25 residual connections, and 6 self-attention operations. The network also takes the noise scheduler ($\bar{\gamma}_t$)

Algorithm 1 Conditional Diffusion Model Pre-Training

Require: $x_0 \sim$ fully sampled images
 $x_{cond} \sim$ Zero Filling Reconstruction($A^H y$)
Network \mathfrak{N}_θ to be optimized

- 1: **while** not converged **do**
- 2: $t \sim \text{DiscreteU}(1, T)$
- 3: $\varepsilon \sim \mathcal{N}(0, I)$
- 4: $\alpha_t = \sqrt{\bar{\gamma}_t}$, $\sigma_t = \sqrt{1 - \bar{\gamma}_t}$
- 5: $v = \alpha_t \varepsilon - \sigma_t x_0$
- 6: Gradient descent on:
$$\nabla_\theta \|\mathfrak{N}_\theta(x_{cond}, \alpha_t x_0 + \sigma_t \varepsilon, \bar{\gamma}_t) - v\|$$
- 7: **end while**

as its third input, which was encoded using a simple three-layer multi-layer perceptron, inspired by previous works [45] focusing on conditional generation.

In this work, the network is designed to predict a latent variable $v = \sqrt{\bar{\gamma}_t} \varepsilon - \sqrt{1 - \bar{\gamma}_t} x_0$, which is better suited for distillation [44], considering the fact that the standard noise prediction parameterization used in DDPM is not well suited for distillation, particularly as the signal-to-noise ratio (SNR) approaches zero, where small errors in noise prediction can be significantly amplified, leading to unstable training and degraded performance. Moreover, when distilling down to very few sampling steps, the connection between noise prediction and data reconstruction becomes unreliable. Using the v -diffusion parameterization, the denoising process turns into $\hat{x}_0 = \alpha_t x_t - \sigma_t \mathfrak{N}_\theta$, which better preserves stable supervision signals during distillation and enables more efficient sampling. Following this modification, progressive distillation is then carried out iteratively to achieve robust image reconstruction to achieve one-step reconstruction. In each distillation iteration, the student model is optimized to halve the overall sampling steps T to $T/2$ by learning to replicate the behavior of two sampling steps of the teacher model in just one step, as detailed in **Algorithm 2**.

C. SSDM-MRI for multi-coil data and QSM acceleration

Similar to our previous work [15], the reconstruction of SSDM-MRI for multi-coil data can be carried out as follows: (1) zero-filling reconstruction was first performed for each receiver channel, (2) then, nm the coil sensitivity maps were estimated using the POEM method for coil combination [47], (3) next, the combined images were fed into SSDM-MRI network (without data consistency) for initial reconstruction, (4) then the initial reconstructions were multiplied by the estimated coil sensitivities to convert back into a multi-channel k-space, (5) finally, data consistency was conducted for every coil to obtain images for each coil channel. Finally, these multi-coil images were re-combined using the POEM method [47].

Although the proposed SSDM-MRI is designed for 2D MRI reconstructions, it can be easily transferred to advanced 3D MRI-based applications in a slice-by-slice manner with proper 1D Fourier Transform preprocessing and k-space data consistency, if the acquisition follows the strategy proposed in our previous QSM acceleration work [15]. iQSM+ [48]

Algorithm 2 Iterative Distillation

Require: \mathfrak{N}_η : pre-trained teacher model (T steps)
 \mathfrak{N}_θ : student model,
Dataset: $\{x_0^n, x_{cond}^n\}$, $n = 1, 2, 3 \dots N$

- 1: **for** n in range(N) **do**
- 2: Initialize \mathfrak{N}_θ from \mathfrak{N}_η
- 3: **while** not converged **do**
- 4: $t \sim \text{DiscreteU}(1, T/2) \times 2$
- 5: $\varepsilon \sim \mathcal{N}(0, I)$
- 6: $t_1 = t - 1$, $t_2 = t - 2$
- 7: $x_t = \alpha_t x_0^n + \sigma_t \varepsilon$
- 8: $x_0 = \alpha_t x_t - \sigma_t \mathfrak{N}_\eta(x_{cond}^n, x_t, \bar{\gamma}_t)$
- 9: $x_{t_1} = \alpha_{t_1} x_0 + \frac{\sigma_{t_1}}{\sigma_t} (x_t - \alpha_t x_0)$
- 10: $x_0'' = \alpha_{t_1} x_{t_1} - \sigma_{t_1} \mathfrak{N}_\eta(x_{cond}^n, x_{t_1}, \bar{\gamma}_{t_1})$
- 11: $\varepsilon_{t_2} = \frac{(x_t - \alpha_{t_2} x_0'')}{\sigma_{t_2}}$
- 12: $\hat{v} = \alpha_{t_2} \varepsilon_{t_2} - \sigma_{t_2} x_0''$
- 13: $L_\theta = \|\mathfrak{N}_\theta(x_{cond}^n, x_t, \bar{\gamma}_{t_2}) - \hat{v}\|_2^2$ \triangleright update θ
- 14: **end while**
- 15: $\mathfrak{N}_\theta \Rightarrow \mathfrak{N}_\eta$ \triangleright Make student next teacher
- 16: $T \rightarrow T/2$ \triangleright Sampling steps is halved
- 17: **end for**

was adopted for QSM reconstruction from reconstructed MRI phase images.

D. Training Data Preparation and Network Training

In this work, two different instances of the proposed SSDM-MRI were obtained by using two different types of training datasets, i.e., (1) the public fastMRI brain dataset [34], and (2) an in-house multi-echo gradient echo (mGRE) complex-valued MRI dataset used in our recent work [15]. In this study, except for the QSM-oriented comparative study, all other evaluations were carried out using the one trained on fastMRI data.

Details about these two datasets are as follows:

(1) **fastMRI Brain Dataset** We extracted a total of 34,063 2D brain images (size: 320×320) from 2,610 volumes randomly selected from the fastMRI brain train dataset batch [34]. The last three slices of each volume were discarded to avoid noise-only slices. All the images were linearly normalized (divided by the maximum intensity of the image) before being fed into the network for training. Different undersampling masks of various types (including 1D and 2D Gaussian masks, and 2D Poisson masks under various AFs, i.e., $4 \times$, $6 \times$, $8 \times$, $10 \times$, $12 \times$, and $15 \times$) were randomly simulated at the beginning of every training mini-batch to synthesize subsampled k-space data and the corresponding zero-filling reconstructions.

(2) **mGRE Brain Data** A total of 44,063 complex-valued slices (image size: 256×256) were retrospectively obtained from 47 subjects (Institutional ethics board approvals have been obtained for all MRI-QSM brain data used in this work), which were acquired at 3T (Discovery 750, GE Healthcare, Milwaukee, WI), with the following parameters: 8 unipolar echoes, first TE / Δ TE = 3 ms / 3.3 ms, TR = 29.8 ms, FOV = $256 \times 256 \times 128$, resolution = 1 mm isotropic. The image normalization and subsampled k-space simulation were made the same as the pipeline described for fastMRI brain dataset.

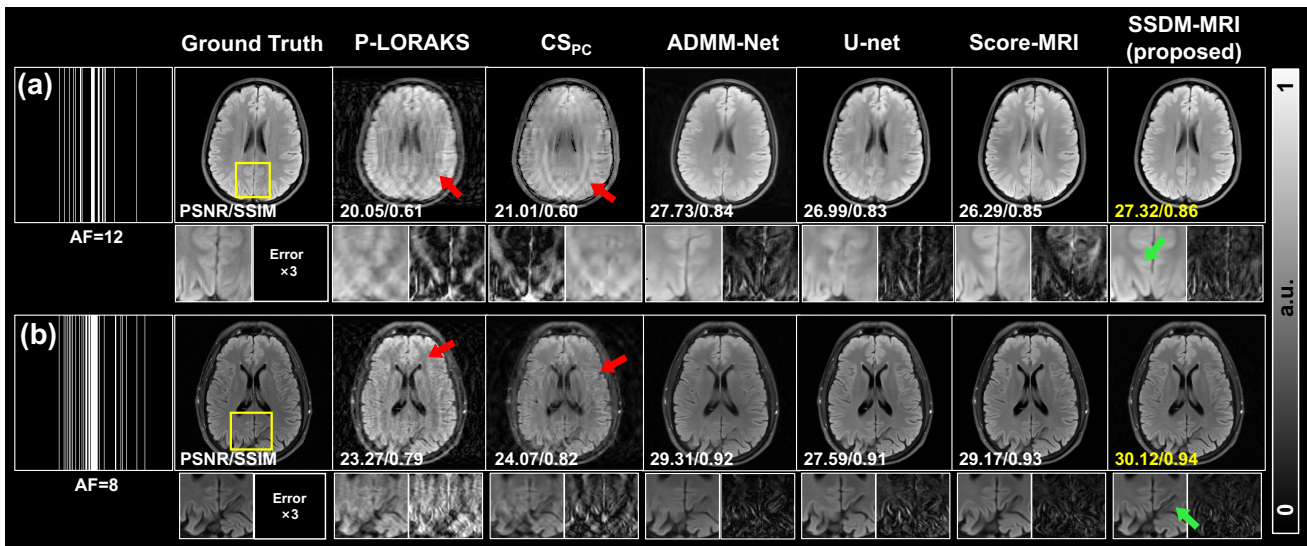


Fig. 2. Comparison of SSDM-MRI with various reconstruction methods on two single-coil brain slices. (a) and (b) demonstrates the results under acceleration factors of 12 (1D Gaussian, ACS = 6 lines) and 8 (1D Gaussian, ACS = 12 lines), respectively. Red arrows point to the reconstruction errors in P-LORAKS and CS_{PC}, while green arrow in the zoomed-in image indicates improved fine details in SSDM-MRI.

All network training were conducted on two NVIDIA V100 (32 GB) GPUs, based on the loss functions defined in **Algorithm 1 and 2**. For DM pretraining, all learnable parameters in the network were initialized as random numbers with a mean of 1 and standard deviation of 0.001, and are optimized using the Adam optimizer with a learning rate of 5×10^{-5} for 200 epochs. The proposed models were implemented using Pytorch 1.13.1. The source codes and the trained models are available at <https://github.com/YangGaoUQ/SSDM-MRI>.

IV. EXPERIMENTS

A. Evaluation Datasets

The performance and generalization capability of the proposed SSDM-MRI were comprehensively evaluated on the following retrospectively and prospectively undersampled data, including:

- (1) 128 in distribution single-coil brain slices from fastMRI at acceleration factors (AF) of 8 and 12 (1D Gaussian subsampling, ACS = 12 and 6 lines, respectively).
- (2) Out-of-distribution (OOD) fastMRI knee dataset (156 single-coil images) at AF of $12 \times$ (Gaussian 2D).
- (3) A single-coil pathological slice containing brain lesions (AF = $8 \times$), simulated from a subject acquired at 3T using the parameters of the mGRE brain training dataset.
- (4) Retrospective multi-coil brain (78 images at AF=12) and multi-coil knee (103 images at AF=15) datasets with ground truths.
- (5) Two 12-coil prospectively undersampled brain and knee slices (AF = $8 \times$ and $4 \times$) randomly selected from fastMRI testing dataset.
- (6) A brain data (size: $256 \times 256 \times 128 \times 8$) retrospectively undersampled at AF = 8 using sampling masks adopted in [15] to evaluate SSDM-MRI's performance on advanced QSM acceleration task.

B. Performance Evaluation and Numerical Metrics

SSDM-MRI was compared with the two traditional algorithms and three deep learning methods: (1) scan-specific P-LORAKS [49], (2) Compressed Sensing with Phase Cycling (CS_{PC}) [40], (3) the unrolling-based ADMM-Net [17], (4) end-to-end U-net based method [16], and (5) DM-based Score-based MRI [26], [29] ($T = 1000$ overall sampling steps) on the above described datasets of different acceleration factors and subsampling patterns. The deep learning methods were re-trained using the same datasets that were originally used for training the SSDM-MRI. The reconstruction times of different methods on a image of size 320×320 are summarized in Table I, indicating that the reconstruction speed of SSDM-MRI is much faster than that of Score-MRI, since only one reverse step is needed.

Performance evaluation experiments are carried out as follows: (1) The proposed SSDM-MRI was first compared with other reconstruction methods using the single-coil fastMRI brain dataset. (2) Then, it was tested on OOD fastMRI knee images and the simulated pathological lesion brain image to test its generalization capability. (3) Next, SSDM-MRI's performances were further validated on both the retrospective and prospective multi-coil fastMRI data. (4) In addition, SSDM-MRI's performance was evaluated on one 8-echo GRE brain for QSM acceleration following [15], which could compare various methods at the whole brain level instead of a single 2D slice, and evaluate their capability of preserving latent susceptibility information. (5) One more simulated study was

TABLE I
RECONSTRUCTION TIMES OF DIFFERENT METHODS ON A BRAIN IMAGE OF 320×320 SIZE.

P-LORAKS	CC _{PC}	ADMM-Net	U-net	Score-MRI	SSDM-MRI
2.67 s	221.45 s	1.91 s	0.36 s	315.18 s	0.45 s

P-LORAKS and CS_{PC} were run on a Intel i5-12400 CPU Processor, while the other deep learning method were evaluated on a NVIDIA 3060 GPU.

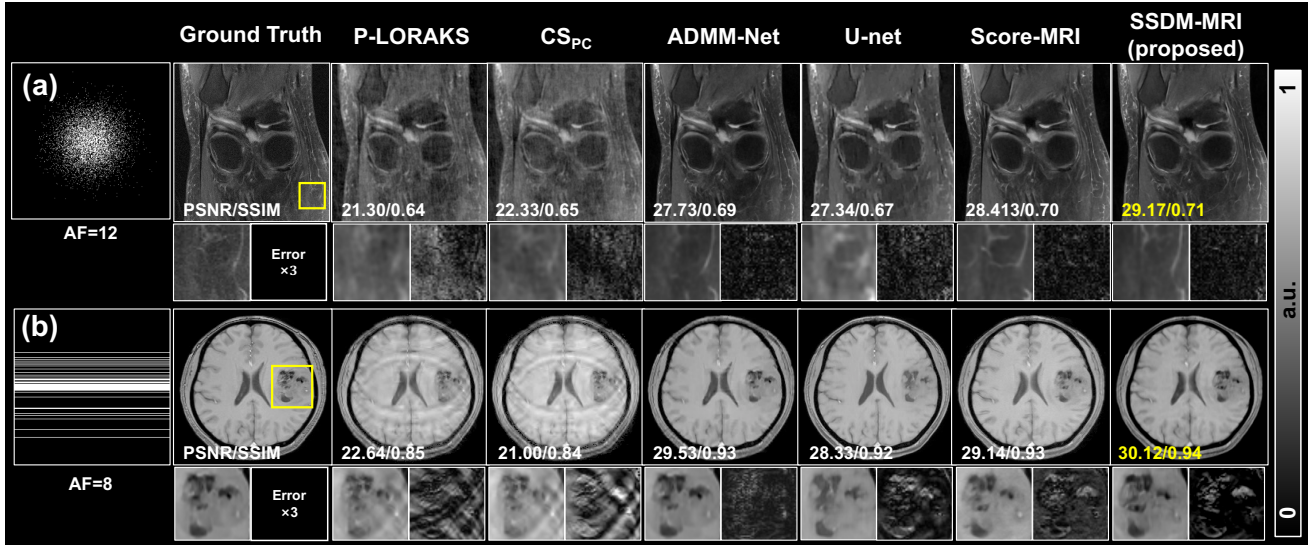


Fig. 3. Comparison of SSDM-MRI with P-LORAKES, CS_{PC}, ADMM-Net, U-net, and Score-MRI, on two slices from (a) fastMRI knee volume at AF = 12 and (b) a pathological subject with severe brain lesions of AF = 8, respectively. Zoomed-in regions and the corresponding error maps were reported below the reconstruction results. The green arrow points to better image fine details in SSDM-MRI.

carried out to investigate the performance of SSDM-MRI against various acceleration factors (AF = 4×, 6×, 8×, 10×, 12×, respectively). (6) Finally, the stability of SSDM-MRI was compared with Score-MRI by inspecting the generation of uncertainty maps.

Peak Signal to Noise Ratio (PSNR) and Structural Similarity (SSIM) [50] were reported for quantitative assessments of different methods on magnitude images, while PSNR and XSIM (a QSM-specific SSIM variants) [51] were reported for the QSM acceleration task. In addition, voxel-wise linear regressions on QSM values of Substantia Nigra (SN) and Red Nucleus (RN) regions were carried out to compare different methods.

V. RESULTS

A. Evaluation on single-coil retrospective data

Fig. 2 compares SSDM-MRI with various MRI accelerating methods on two in-distribution fastMRI single-coil brain slices (AF = 12 and 8, respectively). Overall, SSDM-MRI showed the highest PSNR and SSIM on both datasets, and the minimum errors in the zoomed-in region. P-LORAKS and CS_{PC} showed substantial residual artifacts (red arrows), which are absent in Score-MRI and SSDM-MRI. Meanwhile, SSDM-MRI preserved finer structures (green arrows) compared with other methods.

SSDM-MRI's performance is evaluated on two OOD images (i.e., a fastMRI knee and a pathological brain) in Fig. 3. SSDM-MRI resulted in the minimum error maps and the best fine image details for the knee slice, as pointed out by the green arrow. For the pathological brain image, SSDM-MRI

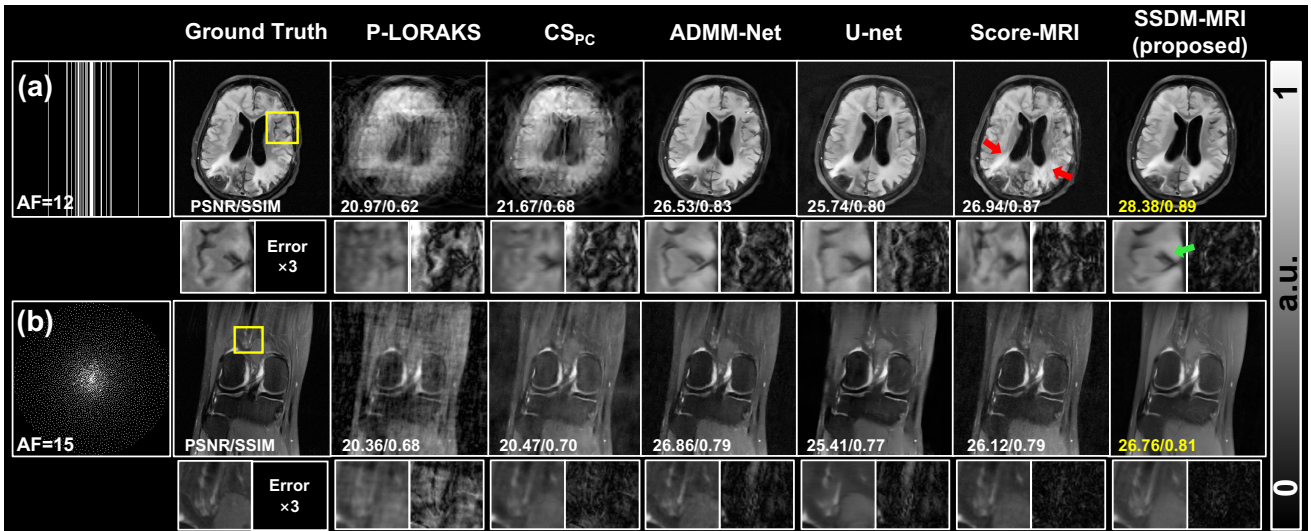


Fig. 4. Comparison of different MRI accelerating methods on two multi-coil data from fastMRI at AF = 12 and 15, respectively. Red arrows point to the residual artifacts in Score-MRI, while green arrow points to the details preserved in SSDM-MRI.

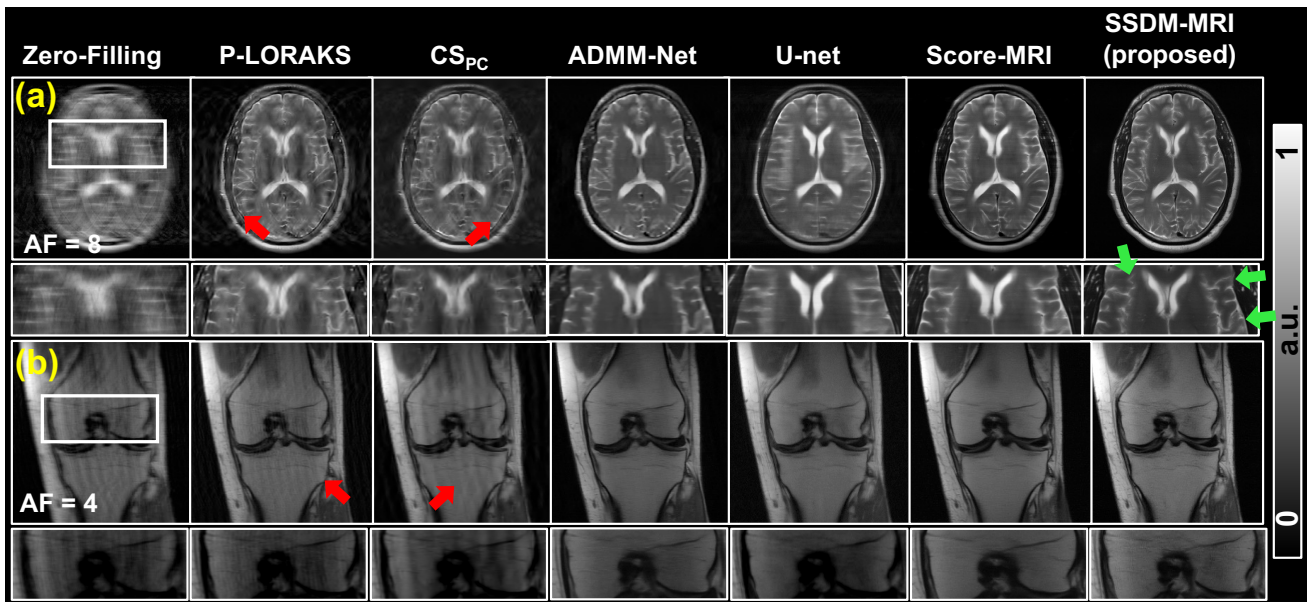


Fig. 5. Comparison of different reconstruction methods on fastMRI brain and knee data, prospectively undersampled at AF=8 and AF=4, respectively. Red arrows point to artifacts and residual artifacts in ADMM-Net, while green arrows point to better image fine structures in SSDM-MRI.

led to the best metrics among all methods, while ADMM-Net led to the minimum error map on the brain lesion.

B. Evaluation on multi-coil fastMRI data

1) Evaluation on retrospective data:

The proposed SSDM-MRI is compared with P-LORAKS, CS_{PC} , ADMM-Net, U-net, and Score-MRI on two retrospective fastMRI brain and knee images (12-coil) were compared in Fig. 4 at AF = 12 and 15, respectively. P-LORAKS and CS_{PC} led to apparent artifacts and reconstruction errors at these high AFs, while U-net resulted in over-smoothed results. SSDM-MRI not only led to the best numerical metrics but also showed the best fine structures (green arrows), compared with other methods.

Table II summarizes the performances of different methods on four retrospective dataset obtained from fastMRI: (1) single-coil brain, (2) single-coil knee, (3) multi-coil brain, and (4) multi-coil knee images at different AFs and different types of sampling masks. SSDM-MRI achieved on average the best PSNR and SSIMs in nearly all situations, compared with the other algorithms.

2) Evaluation on prospective data:

Different methods for two prospectively undersampled data are compared in Fig. 5. Similar to the simulation case, traditional algorithms, i.e., P-LORAKS, CS_{PC} demonstrated substantial artifacts (red arrows), which were successfully removed by ADMM-Net, U-net, Score-MRI, and SSDM-MRI. In addition, SSDM-MRI also significantly reduced the image

TABLE II
COMPARISON OF DIFFERENT MRI METHODS ON THE FOUR RETROSPECTIVE FASTMRI DATASETS IN TERMS OF PSNR AND SSIM.

		P-LORAKS	CS_{PC}	ADMM-NET	U-net	Score-MRI	SSDM-MRI
Single-coil knee (156 images)	Gaussian 2D ×8	25.94 ± 2.031 0.76 ± 0.047	25.56 ± 2.074 0.76 ± 0.044	27.94 ± 2.343 0.79 ± 0.043	27.46 ± 2.265 0.79 ± 0.056	29.95 ± 2.144 0.81 ± 0.071	29.49 ± 2.213 0.82 ± 0.067
	Gaussian 1D ×12	21.74 ± 1.754 0.56 ± 0.081	21.27 ± 1.337 0.54 ± 0.076	27.56 ± 2.318 0.77 ± 0.023	25.96 ± 2.866 0.75 ± 0.085	28.19 ± 2.879 0.76 ± 0.023	28.08 ± 2.311 0.78 ± 0.043
Single-coil brain (128 images)	Gaussian 1D ×8	25.34 ± 1.613 0.82 ± 0.049	25.11 ± 1.431 0.82 ± 0.062	32.93 ± 2.557 0.92 ± 0.017	31.71 ± 2.808 0.91 ± 0.038	32.77 ± 1.995 0.92 ± 0.024	33.83 ± 2.311 0.93 ± 0.029
	Poisson 2D ×15	24.77 ± 1.983 0.70 ± 0.061	24.54 ± 2.454 0.69 ± 0.051	29.11 ± 2.353 0.86 ± 0.037	28.98 ± 1.967 0.84 ± 0.066	29.29 ± 2.348 0.88 ± 0.038	30.19 ± 2.103 0.89 ± 0.034
Multi-coil brain (78 images)	Gaussian 1D ×12	21.45 ± 1.217 0.63 ± 0.084	20.71 ± 1.146 0.63 ± 0.078	28.15 ± 2.254 0.85 ± 0.024	27.71 ± 2.365 0.83 ± 0.028	29.59 ± 1.897 0.89 ± 0.047	31.28 ± 2.314 0.90 ± 0.031
	Random 1D ×12	20.41 ± 1.943 0.54 ± 0.074	19.85 ± 2.575 0.53 ± 0.066	26.14 ± 2.154 0.78 ± 0.061	25.42 ± 2.993 0.77 ± 0.083	26.67 ± 2.079 0.85 ± 0.053	27.66 ± 2.473 0.86 ± 0.041
Multi-coil knee (103 images)	Poisson 2D ×15	23.67 ± 2.185 0.62 ± 0.072	22.57 ± 2.553 0.63 ± 0.063	28.31 ± 2.438 0.75 ± 0.087	27.98 ± 2.567 0.74 ± 0.076	29.35 ± 2.379 0.77 ± 0.073	29.89 ± 2.132 0.78 ± 0.067
	Gaussian 1D ×12	20.31 ± 2.743 0.55 ± 0.078	20.15 ± 2.677 0.54 ± 0.076	26.71 ± 2.791 0.73 ± 0.074	26.42 ± 2.990 0.71 ± 0.083	27.97 ± 2.673 0.78 ± 0.053	29.01 ± 2.510 0.78 ± 0.057

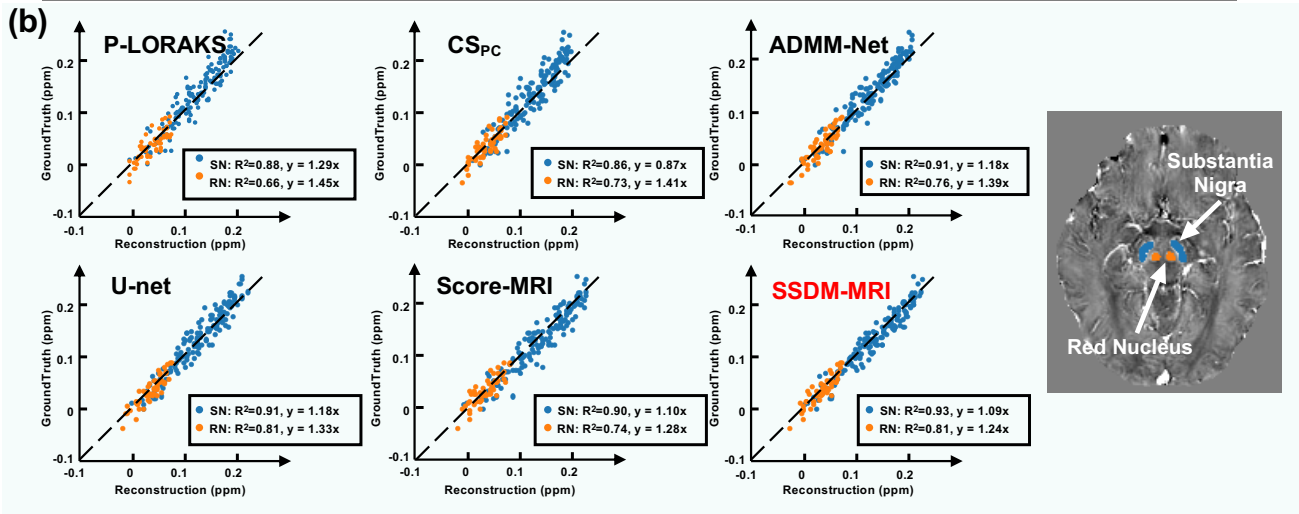
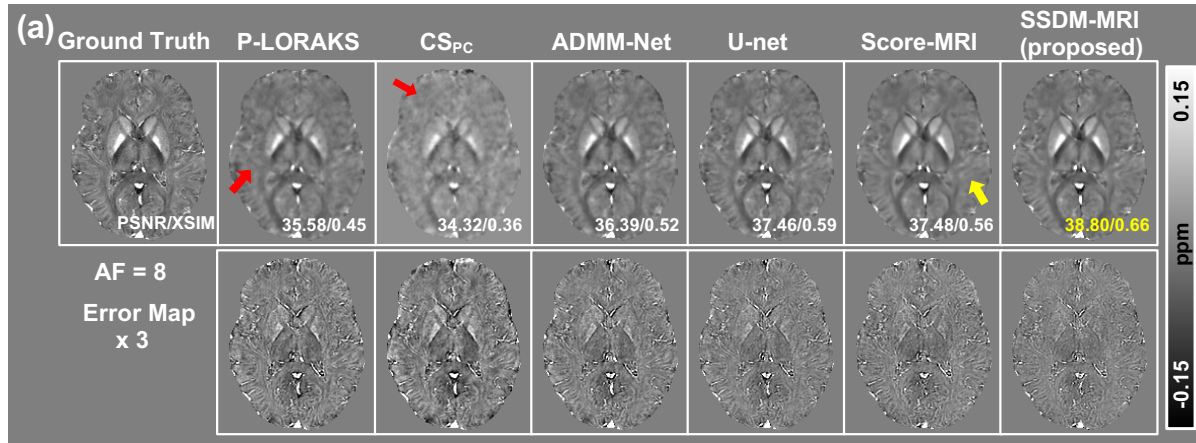


Fig. 6. Comparison of the proposed SSDM-MRI with other accelerating methods on one QSM subject, retrospectively subsampled at AF = 8. (a) demonstrates the computed QSM images and corresponding error maps. Red arrows point to artifacts in P-LORAKES, CS_{PC}, while yellow arrows point to over-smoothing in Score-MRI. (b) shows the scatter plots of susceptibility measurements in two deep grey matter regions (Substantia Nigra (SN) and Red Nucleus (RN)) of various methods (x-axis) against the ground truth (y-axis). Linear regression results are reported correspondingly.

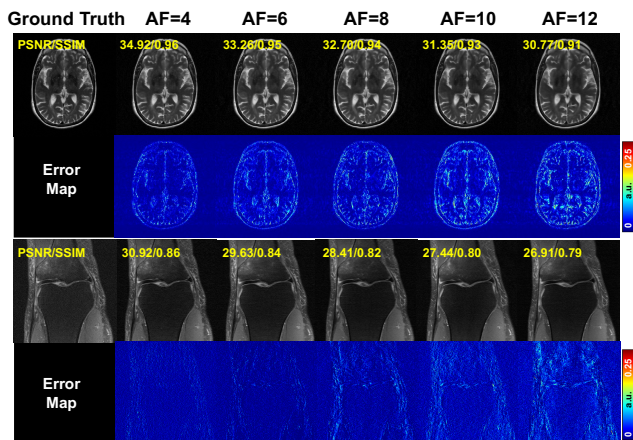


Fig. 7. Performance evaluation of the proposed SSDM-MRI against various accelerating rates from AF = 4 to 12, with PSNR and SSIM reported at the top part of the reconstructed brain and knee images.

blurring apparent in U-net and demonstrated the best fine structures as pointed out by the green arrows.

C. Comparison on QSM acceleration task

Fig. 6 compares different methods on a QSM brain volume at 8× acceleration. While all methods showed dramatic detail loss, compared to the fully-sampled QSM ground truth. SSDM-MRI resulted in the minimum error map and the best PSNR and XSIM (38.80 and 0.66). Linear regression was also performed on susceptibility values of various reconstruction methods against those of the ground truth, as shown Fig. 6(b). It confirmed that the proposed SSDM-MRI achieved the most accurate quantitative measurements in both SN ($R^2 = 0.93$) and RN ($R^2 = 0.81$) regions.

D. The effects of accelerating factors

The reconstructions of SSDM-MRI under 5 different AFs are shown in Fig. 7, on one retrospectively subsampled brain and a knee image. None of the reconstructed images showed apparent artifacts; however, as the AFs increases, more fine details gradually became blurred, which was also confirmed in the error maps.

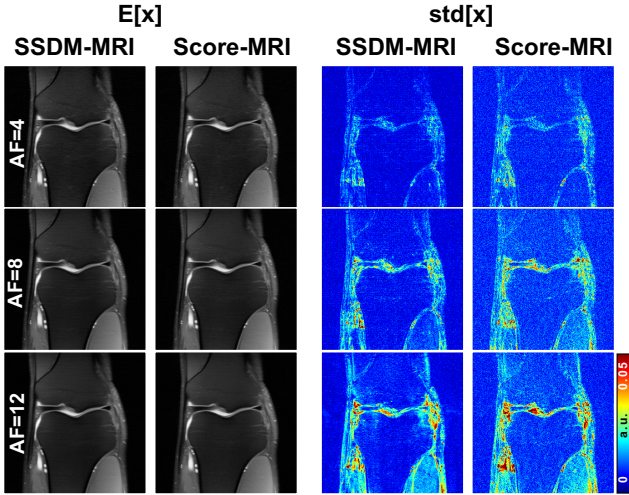


Fig. 8. The uncertainty maps of SSDM-MRI and Score-MRI on one knee slice at accelerating rates of $4\times$, $8\times$, and $12\times$, respectively. The left panel demonstrates the average results of 5 times repetitive reconstructions starting from various Gaussian noise, while the right panel shows the corresponding standard deviations.

E. Reconstruction stability of SSDM-MRI

Fig. 8 illustrates the uncertainty maps of SSDM-MRI and Score-MRI of 5 repetitive reconstructions on one knee slice at $AF = 4\times$, $8\times$, $12\times$ respectively. As the AF increases from 4 to 12, both DM-based methods exhibited a notable increase in uncertainty images, with the Score-MRI demonstrating slightly larger standard deviations than the proposed SSDM-MRI.

VI. DISCUSSION AND CONCLUSION

In this work, we demonstrated the feasibility of MRI reconstructions from highly undersampled k-space with only a single-step posterior sampling of a diffusion model (DM). Specifically, an SSDM-MRI framework was constructed by progressively distilling a conventional DM. Extensive comparative studies were carried out to compare the performances of SSDM-MRI with those of multiple existing algorithms, i.e., P-LORAKS [49], CS_{PC} [40], ADMM-Net [17], U-net [16], and DM-based Score-MRI [26] on both public fastMRI images and a private QSM subject. In general, the proposed method exhibited the best results on most images with fewer errors, improved numerical metrics and image fine details, and more accurate susceptibility measurements in the substantia nigra and red nucleus.

There have already been several DM-based methods proposed for MRI acceleration [24]–[31], showing better reconstruction performances, especially when compared with traditional iterative and existing end-to-end deep learning (DL) based methods [12]–[14]. However, the computational costs of DM-based methods are usually much higher than previous DL methods, e.g., U-net-based frameworks, due to the need of a relatively large number of poster sampling steps, making the overall reconstruction time much longer and hindering their applications in clinical practice. To the best of our knowledge, SSDM-MRI is the first single-step DM-based method, whose reconstruction time is comparable to the end-to-end deep neural networks, as evident in Table I.

In this work, the proposed SSDM-MRI demonstrated promising generalization capability on the OOD knee data, despite the fact that it was trained on brain images only, demonstrating SSDM-MRI’s ability to learn the conditional prior underlaid in shared anatomical and statistical patterns of brain and knee images instead of simply memorizing the features. Although the adaptability of SSDM-MRI may not be as good as fully unsupervised methods (e.g., the slight performance decrease in Tabel II for knee images), it still demonstrates great robustness across vairous anatomies.

In the QSM experiment, different methods were repetitively tested on 1024 (128 slice number \times 8 echo number) consecutive 2D images, covering the whole brain before QSM reconstructions from MRI phases. The proposed SSDM-MRI not only achieved on average the best results for all brain slices, but also preserved the best slice-to-slice coherence. It also resulted in the best QSM measurements, demonstrating its capability of preserving latent and weak susceptibility signal buried in the MRI phase images.

SSDM-MRI’s performances were also evaluated against varying accelerating rates, and the results showed that no substantial artifacts were introduced. However, the image quality also gradually degraded with increasing AFs, and in the future, we will continue working on obtaining high-quality images with high AFs. In addition, the reconstruction stability also needs to be further optimized to obtain more reliable solutions.

In conclusion, this study proposed a single-step diffusion model(DM)-based method, SSDM-MRI, for MR image reconstruction from highly undersampled k-space data, via a one-step posterior sampling from a conditional DM. Experimental results demonstrated that SSDM-MRI consistently led to improved results compared with several state-of-the-art methods on both magnitude and QSM reconstruction tasks, respectively, in a much shorter reconstruction time.

REFERENCES

- [1] G. B. Frisoni, N. C. Fox, C. R. Jack Jr, P. Scheltens, and P. M. Thompson, “The clinical use of structural mri in alzheimer disease,” *Nature reviews neurology*, vol. 6, no. 2, pp. 67–77, 2010.
- [2] À. Rovira, M. P. Wattjes, M. Tintoré, C. Tur, T. A. Youstry, M. P. Sormani, N. De Stefano, M. Filippi, C. Auger, M. A. Rocca *et al.*, “Magnims consensus guidelines on the use of mri in multiple sclerosis—clinical implementation in the diagnostic process,” *Nature Reviews Neurology*, vol. 11, no. 8, pp. 471–482, 2015.
- [3] M. Lustig, D. Donoho, and J. M. Pauly, “Sparse mri: The application of compressed sensing for rapid mr imaging,” *Magnetic Resonance in Medicine*, vol. 58, no. 6, pp. 1182–1195, 2007.
- [4] M. Lustig, D. L. Donoho, J. M. Santos, and J. M. Pauly, “Compressed sensing mri,” *IEEE signal processing magazine*, vol. 25, no. 2, pp. 72–82, 2008.
- [5] M. Doneva, P. Börnert, H. Eggers, C. Stehning, J. Sénégas, and A. Mertins, “Compressed sensing reconstruction for magnetic resonance parameter mapping,” *Magnetic resonance in medicine*, vol. 64, no. 4, pp. 1114–1120, 2010.
- [6] Y. Yang, F. Liu, W. Xu, and S. Crozier, “Compressed sensing mri via two-stage reconstruction,” *IEEE Transactions on biomedical engineering*, vol. 62, no. 1, pp. 110–118, 2014.
- [7] Y. Yang, F. Liu, Z. Jin, and S. Crozier, “Aliasing artefact suppression in compressed sensing mri for random phase-encode undersampling,” *IEEE Transactions on Biomedical Engineering*, vol. 62, no. 9, pp. 2215–2223, 2015.

- [8] K. H. Jin, D. Lee, and J. C. Ye, "A general framework for compressed sensing and parallel mri using annihilating filter based low-rank hankel matrix," *IEEE Transactions on Computational Imaging*, vol. 2, no. 4, pp. 480–495, 2016.
- [9] S. G. Lingala, Y. Hu, E. DiBella, and M. Jacob, "Accelerated dynamic mri exploiting sparsity and low-rank structure: kt slr," *IEEE transactions on medical imaging*, vol. 30, no. 5, pp. 1042–1054, 2011.
- [10] T. Zhang, J. M. Pauly, and I. R. Levesque, "Accelerating parameter mapping with a locally low rank constraint," *Magnetic resonance in medicine*, vol. 73, no. 2, pp. 655–661, 2015.
- [11] S. Ravishankar, J. C. Ye, and J. A. Fessler, "Image reconstruction: From sparsity to data-adaptive methods and machine learning," *Proceedings of the IEEE*, vol. 108, no. 1, pp. 86–109, 2019.
- [12] C. M. Hyun, H. P. Kim, S. M. Lee, S. Lee, and J. K. Seo, "Deep learning for undersampled mri reconstruction," *Physics in Medicine & Biology*, vol. 63, no. 13, p. 135007, 2018.
- [13] S. Shan, Y. Gao, P. Z. Liu, B. Whelan, H. Sun, B. Dong, F. Liu, and D. E. Waddington, "Distortion-corrected image reconstruction with deep learning on an mri-linac," *Magnetic resonance in medicine*, vol. 90, no. 3, pp. 963–977, 2023.
- [14] P. Guo, Y. Mei, J. Zhou, S. Jiang, and V. M. Patel, "Reconformer: Accelerated mri reconstruction using recurrent transformer," *IEEE transactions on medical imaging*, vol. 43, no. 1, pp. 582–593, 2023.
- [15] Y. Gao, M. Cloos, F. Liu, S. Crozier, G. B. Pike, and H. Sun, "Accelerating quantitative susceptibility and r2* mapping using incoherent undersampling and deep neural network reconstruction," *NeuroImage*, vol. 240, p. 118404, 2021.
- [16] O. Ronneberger, P. Fischer, and T. Brox, "U-net: Convolutional networks for biomedical image segmentation," in *Medical image computing and computer-assisted intervention—MICCAI 2015: 18th international conference, Munich, Germany, October 5–9, 2015, proceedings, part III 18*. Springer, 2015, pp. 234–241.
- [17] Y. Yang, J. Sun, H. Li, and Z. Xu, "Deep adm-net for compressive sensing mri," in *Proceedings of the 30th international conference on neural information processing systems*, 2016, pp. 10–18.
- [18] J. Zhang and B. Ghanem, "Ista-net: Interpretable optimization-inspired deep network for image compressive sensing," in *Proceedings of the IEEE conference on computer vision and pattern recognition*, 2018, pp. 1828–1837.
- [19] J. Ho, A. Jain, and P. Abbeel, "Denoising diffusion probabilistic models," *Advances in neural information processing systems*, vol. 33, pp. 6840–6851, 2020.
- [20] Y. Song, J. Sohl-Dickstein, D. P. Kingma, A. Kumar, S. Ermon, and B. Poole, "Score-based generative modeling through stochastic differential equations," *arXiv preprint arXiv:2011.13456*, 2020.
- [21] P. Dhariwal and A. Nichol, "Diffusion models beat gans on image synthesis," *Advances in neural information processing systems*, vol. 34, pp. 8780–8794, 2021.
- [22] A. Q. Nichol and P. Dhariwal, "Improved denoising diffusion probabilistic models," in *International conference on machine learning*. PMLR, 2021, pp. 8162–8171.
- [23] J. Song, C. Meng, and S. Ermon, "Denoising diffusion implicit models," *arXiv preprint arXiv:2010.02502*, 2020.
- [24] J. Chu, C. Du, X. Lin, X. Zhang, L. Wang, Y. Zhang, and H. Wei, "Highly accelerated mri via implicit neural representation guided posterior sampling of diffusion models," *Medical Image Analysis*, vol. 100, p. 103398, 2025.
- [25] W. Bian, A. Jang, L. Zhang, X. Yang, Z. Stewart, and F. Liu, "Diffusion modeling with domain-conditioned prior guidance for accelerated mri and qmri reconstruction," *IEEE Transactions on Medical Imaging*, 2024.
- [26] H. Chung and J. C. Ye, "Score-based diffusion models for accelerated mri," *Medical image analysis*, vol. 80, p. 102479, 2022.
- [27] C. Cao, Z.-X. Cui, Y. Wang, S. Liu, T. Chen, H. Zheng, D. Liang, and Y. Zhu, "High-frequency space diffusion model for accelerated mri," *IEEE Transactions on Medical Imaging*, 2024.
- [28] Y. Liu, Z.-X. Cui, S. Qin, C. Liu, H. Zheng, H. Wang, Y. Zhou, D. Liang, and Y. Zhu, "Score-based diffusion models with self-supervised learning for accelerated 3d multi-contrast cardiac mr imaging," *IEEE Transactions on Medical Imaging*, 2025.
- [29] H. Chung, J. Kim, M. T. Mccann, M. L. Klasky, and J. C. Ye, "Diffusion posterior sampling for general noisy inverse problems," *arXiv preprint arXiv:2209.14687*, 2022.
- [30] Z.-X. Cui, C. Cao, Y. Wang, S. Jia, J. Cheng, X. Liu, H. Zheng, D. Liang, and Y. Zhu, "Spirit-diffusion: Self-consistency driven diffusion model for accelerated mri," *IEEE Transactions on Medical Imaging*, 2024.
- [31] L. Chen, X. Tian, J. Wu, R. Feng, G. Lao, Y. Zhang, H. Liao, and H. Wei, "Joint coil sensitivity and motion correction in parallel mri with a self-calibrating score-based diffusion model," *Medical Image Analysis*, vol. 102, p. 103502, 2025.
- [32] W. Jiang, Z. Xiong, F. Liu, N. Ye, and H. Sun, "Fast controllable diffusion models for undersampled mri reconstruction," in *2024 IEEE International Symposium on Biomedical Imaging (ISBI)*. IEEE, 2024, pp. 1–5.
- [33] H. Askari, F. Roosta, and H. Sun, "Training-free medical image inverses via bi-level guided diffusion models," in *2025 IEEE/CVF Winter Conference on Applications of Computer Vision (WACV)*. IEEE, 2025, pp. 75–84.
- [34] J. Zbontar, F. Knoll, A. Sriram, T. Murrell, Z. Huang, M. J. Muckley, A. Defazio, R. Stern, P. Johnson, M. Bruno *et al.*, "fastmri: An open dataset and benchmarks for accelerated mri," *arXiv preprint arXiv:1811.08839*, 2018.
- [35] S. Wang, Z. Su, L. Ying, X. Peng, S. Zhu, F. Liang, D. Feng, and D. Liang, "Accelerating magnetic resonance imaging via deep learning," in *2016 IEEE 13th international symposium on biomedical imaging (ISBI)*. IEEE, 2016, pp. 514–517.
- [36] Y. Korkmaz, T. Cukur, and V. M. Patel, "Self-supervised mri reconstruction with unrolled diffusion models," in *International Conference on Medical Image Computing and Computer-Assisted Intervention*. Springer, 2023, pp. 491–501.
- [37] L. Feng, T. Benkert, K. T. Block, D. K. Sodickson, R. Otazo, and H. Chandarana, "Compressed sensing for body mri," *Journal of Magnetic Resonance Imaging*, vol. 45, no. 4, pp. 966–987, 2017.
- [38] M. Hong, Y. Yu, H. Wang, F. Liu, and S. Crozier, "Compressed sensing mri with singular value decomposition-based sparsity basis," *Physics in Medicine & Biology*, vol. 56, no. 19, p. 6311, 2011.
- [39] K. Hammernik, T. Klatzer, E. Kobler, M. P. Recht, D. K. Sodickson, T. Pock, and F. Knoll, "Learning a variational network for reconstruction of accelerated mri data," *Magnetic resonance in medicine*, vol. 79, no. 6, pp. 3055–3071, 2018.
- [40] F. Ong, J. Y. Cheng, and M. Lustig, "General phase regularized reconstruction using phase cycling," *Magnetic resonance in medicine*, vol. 80, no. 1, pp. 112–125, 2018.
- [41] F. Zhao, D. C. Noll, J.-F. Nielsen, and J. A. Fessler, "Separate magnitude and phase regularization via compressed sensing," *IEEE transactions on medical imaging*, vol. 31, no. 9, pp. 1713–1723, 2012.
- [42] Y. Song, L. Shen, L. Xing, and S. Ermon, "Solving inverse problems in medical imaging with score-based generative models," *arXiv preprint arXiv:2111.08005*, 2021.
- [43] Y. Song, P. Dhariwal, M. Chen, and I. Sutskever, "Consistency models," *arXiv preprint arXiv:2303.01469*, 2023.
- [44] T. Salimans and J. Ho, "Progressive distillation for fast sampling of diffusion models," *arXiv preprint arXiv:2202.00512*, 2022.
- [45] C. Saharia, W. Chan, H. Chang, C. Lee, J. Ho, T. Salimans, D. Fleet, and M. Norouzi, "Palette: Image-to-image diffusion models," in *ACM SIGGRAPH 2022 conference proceedings*, 2022, pp. 1–10.
- [46] J. Schlemper, J. Caballero, J. V. Hajnal, A. N. Price, and D. Rueckert, "A deep cascade of convolutional neural networks for dynamic mr image reconstruction," *IEEE transactions on Medical Imaging*, vol. 37, no. 2, pp. 491–503, 2017.
- [47] H. Sun, J. O. Cleary, R. Glarin, S. C. Kolbe, R. J. Ordidge, B. A. Moffat, and G. B. Pike, "Extracting more for less: multi-echo mp2rage for simultaneous t1-weighted imaging, t1 mapping, mapping, swi, and qsm from a single acquisition," *Magnetic resonance in medicine*, vol. 83, no. 4, pp. 1178–1191, 2020.
- [48] Y. Gao, Z. Xiong, S. Shan, Y. Liu, P. Rong, M. Li, A. H. Wilman, G. B. Pike, F. Liu, and H. Sun, "Plug-and-play latent feature editing for orientation-adaptive quantitative susceptibility mapping neural networks," *Medical Image Analysis*, vol. 94, p. 103160, 2024.
- [49] J. P. Haldar and J. Zhuo, "P-loraks: low-rank modeling of local k-space neighborhoods with parallel imaging data," *Magnetic resonance in medicine*, vol. 75, no. 4, pp. 1499–1514, 2016.
- [50] Z. Wang, A. C. Bovik, H. R. Sheikh, and E. P. Simoncelli, "Image quality assessment: from error visibility to structural similarity," *IEEE transactions on image processing*, vol. 13, no. 4, pp. 600–612, 2004.
- [51] C. Milovic, C. Tejos, J. Silva, K. Shmueli, and P. Irarrazaval, "Xsim: A structural similarity index measure optimized for mri qsm," *Magnetic Resonance in Medicine*, vol. 93, no. 1, pp. 411–421, 2025.